


Absorption and Scattering by a Temporally Switched Lossy Layer: Going beyond the Rozanov Bound

Chen Firestein¹, Amir Shlivinski^{1,*} and Yakir Hadad^{2,†}

¹*School of Electrical and Computer Engineering, Ben-Gurion University of the Negev, Beer Sheva 84105, Israel*

²*School of Electrical Engineering, Tel-Aviv University, Ramat-Aviv, Tel-Aviv 69978, Israel*

 (Received 4 May 2021; revised 30 September 2021; accepted 6 December 2021; published 13 January 2022)

In this paper we study the electromagnetic scattering, absorption, and performance bounds for short time modulated pulses that impinge on a time-varying lossy layer that is sandwiched between vacuum and a perfect electric conductor. The electric characteristics of the layer, namely, the conductivity, permittivity, and permeability, are assumed to change *abruptly or gradually* in time. We demonstrate numerically that a time-varying absorbing layer that undergoes temporal switching of its *permittivity and conductance* can absorb the power of a modulated, ultrawideband, as well as a quasimonochromatic, pulsed wave *beyond* what is dictated by the time-invariant Rozanov bound *when integrating over the whole frequency spectrum*. We suggest and simulate a practical metamaterial realization that is constructed as a three-dimensional array of resistor loaded dipoles. By switching only the dipole's load resistance, desired effective media properties are obtained. Furthermore, we show that Rozanov's bound can be bypassed with abrupt and a more practical gradual, soft, switching, thus overcoming some possible causality issues in abrupt switching.

DOI: [10.1103/PhysRevApplied.17.014017](https://doi.org/10.1103/PhysRevApplied.17.014017)

I. INTRODUCTION

Wave absorbers find important applications in various wave-based systems, in acoustics and electromagnetics, where they are used for the minimization of scattering and emission from certain domains, as for example radar absorbers or in electromagnetic compatibility applications [1–8]. The typical absorber is based on a proper spatial arrangement of linear and time-invariant (LTI) lossy materials. For LTI absorbers that consist of a lossy layer backed by an ideal conductor (a perfect electric conductor), Rozanov [9] developed a fundamental trade-off between the absorber thickness and the absorption bandwidth. However, since this bound, as several other bounds in wave theory, has been developed under the LTI assumption, it does not necessarily apply when non-LTI, e.g., linear time-varying (LTV) wave systems, are considered. In fact, time-varying wave devices have been shown in recent years to allow an additional degree of freedom compared to conventional LTI designs and therefore in many cases they can potentially achieve better performances [10–15]. Interestingly, time variation is also considered a means of wave manipulation, leading to additional peculiar functionalities [16–32].

As spatial variations, temporal variations can also take different forms, such as periodic modulation and temporal discontinuity. The former is better suited for narrowband applications [11,33,34], whereas the latter fits better with pulsed wave applications. Specifically, it has been used in Ref. [10] to achieve better impedance matching between transmission line and reactive loads for short time pulses, in Ref. [29] for the purpose of antireflection coating, and in Ref. [13] to improve the reflection bandwidth of a Dalenbach screen. Furthermore, the problem of reflection and transmission, as well as energy balance, in the presence of abrupt and gradual temporal variation of the guiding medium were explored in Refs. [35–44].

Scattering and radiation by time modulated small obstacles that can be described using the dipole approximation have been explored in Refs. [45–48]. Such descriptions may be helpful for the development of homogenization methodologies for time-varying composite media and may be used to practically emulate effective bulk metamaterials with various time-varying characteristics, as regained, e.g., in our work.

In this paper we study the electromagnetic wave scattering and absorption of short time pulses that impinge on a time-varying lossy dielectric layer that is sandwiched between the half-space of vacuum and a perfect electric conductor. The electric characteristics of the layer, namely, its conductivity, permittivity, and permeability, are assumed to change *abruptly or gradually* in time.

*amirshli@bgu.ac.il

†hadady@eng.tau.ac.il

To make the analysis as general as possible, we study the equivalent transmission line (TL) problem of the actual electromagnetic system. In accordance with Rozanov's bound, the incident pulse is assumed to impinge normally, which enforces a TEM mode [49,50]. We solve a temporally switched TL problem in the complex frequency plane s and, by performing an inverse Laplace transform, the time-domain voltage is obtained for any point along the TL. We use this approach to augment the Rozanov bound for ultrawideband and quasimonochromatic short time pulsed signals followed by a demonstration of how it may be bypassed using a temporally switched layered wave absorber. While our time-domain absorption analysis has a broader applicability, specifically to bypass the LTI bound, we only apply temporal switching to the layer's permittivity and conductivity, which simplifies practical realizations. To that end, we suggest a metamaterial structure that is composed of an array of resistor loaded dipoles. By changing the *resistance only* we obtain the required effective media properties. Moreover, we demonstrate that, by using a realistic gradual soft switching instead of an abrupt one, the absorption of the time-variant system is still better than the Rozanov bound, even if the switching duration is several times larger than the pulse temporal width.

II. DESCRIPTION OF THE PROBLEM

An electromagnetic pulsed wave with electric and magnetic fields, $\vec{E}(\mathbf{r}, t)$ and $\vec{H}(\mathbf{r}, t)$, propagates in vacuum in the normal direction toward an absorbing layer. At $t = t_0$ the pulsed wave impinges a dielectric layer with permittivity, permeability, conductivity, and magnetic conductivity $(\epsilon_1, \mu_1, \sigma_1, \sigma_{m1})$. The layer thickness is d , and it is sandwiched between vacuum and an ideal electric conductor. See Fig. 1(a) for an illustration.

With respect to the plane of incidence, the wave is of a transverse electromagnetic (TEM) mode that enables the use of an equivalent TL model. Following standard textbook formulation, such as Refs. [49,50], the TL model is readily available.

We assume that initially the layer is lossless and can be described by the TL parameters $\{L_1, C_1\}$ ($\{R_1 = 0, G_1 = 0\}$), where $\{L_1, C_1\}$ ($\{R_1, G_1\}$) are the per unit length inductance and capacitance (series resistance and parallel admittance). Because of the spatial discontinuity at $x = 0$, some of the impinging wave will be back reflected upon incidence [see Fig. 1(c)]. This reflection is nondispersive, i.e., the transmitted and back reflected pulses do not change their shape. It has simple reflection coefficients of $\Gamma_s = (Z_1 - Z_0)/(Z_1 + Z_0)$, where $Z_0 = \sqrt{L_0/C_0}$ is the characteristic TL impedance modeling the host medium (vacuum) and $Z_1 = \sqrt{L_1/C_1}$ is the characteristic TL impedance of the layer.

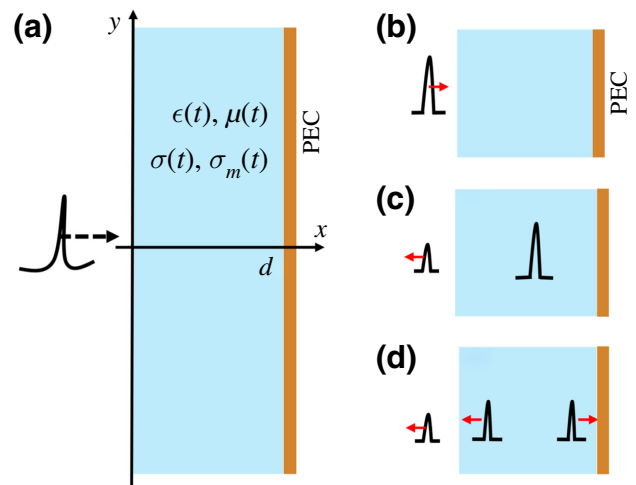


FIG. 1. (a) Problem illustration: a short pulse propagates toward a radar absorber that is composed of a magnetodielectric layer (blue) attached to a perfect electric conductor (PEC) surface (brown). The figure illustrates the (x, y) plane, which is the plane of incidence. (b)–(d) Temporal description of the system. (b) At $t = t_0$ the incident wavefront impinges the boundary. (c) At time $t = t_s$, the wave is completely contained within the layer and an abrupt switching is performed. (d) For times $t > t_s$, the electric and magnetic properties may lead to dispersive reflected and transmitted waves.

At time $t_s > t_0$, while the pulse is completely contained within the layer [see Figs. 1(c) and 1(d)], the TLs' parameters are abruptly switched into a new set of parameters $(\epsilon_2, \mu_2, \sigma_2, \sigma_{m2})$ that translate to $\{L_2, C_2, R_2, G_2\}$ in the TL model, thus forming a *temporal boundary* separating the two TL problems with initial conditions set at $t = t_s^+$ along the TL. In general, this switching process ignites two waves that are counterpropagating inside the layer [51]. These two waves maintain the general pulsed shape; however, their temporal width may be different than that of the pulse at $t < t_s$, giving rise to pulse compression or expansion. In association with that, the switching process may absorb or pump energy into the wave system [10,36].

III. MATHEMATICAL FORMULATION

In this paper we strive to calculate the overall reflection by the temporally switched layer. This includes, of course, the reflection due to the spatial discontinuity at $x = 0$, but it also includes the reflection due to the temporal discontinuity resulting from the switching process, and the energy change caused by it. In order to solve this scattering and absorption problem, in the next section, we develop a time-domain Green's function formalism for the complete analysis of the fields at times $t > t_s$. The wave solution of the pulsed waveform along the layer for $0 < x < d$ and $t > t_s$ is obtained by a superposition integration of Green's

function weighted by an initial time source at $t = t_s^+$ that results from flux continuity conditions.

A. The TL model and its formal solution

We reduce the general plane-wave scattering problem to a one-dimensional (1D) TL problem that is governed by the TL equations

$$\frac{\partial V(x,t)}{\partial x} + L \frac{\partial I(x,t)}{\partial t} + RI(x,t) = 0, \quad (1a)$$

$$\frac{\partial I(x,t)}{\partial x} + C \frac{\partial V(x,t)}{\partial t} + GV(x,t) = 0, \quad (1b)$$

where $V(x,t)$ and $I(x,t)$ denote the voltage and current along the line, respectively, and are related to the field in each domain. As a first step, we transform the time-domain system in Eqs. (1) into the complex frequency (Laplace) domain

$$\frac{\partial V(x,s)}{\partial x} + (sL + R)I(x,s) - LI_0(x) = 0, \quad (2a)$$

$$\frac{\partial I(x,s)}{\partial x} + (sC + G)V(x,s) - CV_0(x) = 0, \quad (2b)$$

where $V_0(x)$ and $I_0(x)$ are the initial voltage and current at $t = t_s^+$, respectively, and s denotes the complex frequency spectral variable. Taking the x derivative of Eq. (2a) followed by the substitution of Eq. (2b) gives the Helmholtz equation for a lossy medium,

$$\frac{\partial^2 V(x,s)}{\partial x^2} - (sL + R)(sC + G)V(x,s) = f_{s,v}(x,s), \quad (3a)$$

$$f_{s,v}(x,s) = L \frac{\partial I_0(x)}{\partial x} - C(sL + R)V_0(x), \quad (3b)$$

with impedance boundary conditions at $x = 0$, and short circuit due to the ideal conductor at $x = d$. We define the spectral Green's function for the voltage, $g_v(x, x', s)$, such that the solution for the spectral voltage $V(x, s)$ can be expressed as the superposition integral

$$V(x, s) = \int_{-\infty}^{\infty} g_v(x, x', s) f_{s,v}(x', s) dx'. \quad (4)$$

From this definition, clearly, $g_v(x, x', s)$ is a solution of

$$\frac{\partial^2 g_v(x, x', s)}{\partial x^2} - \gamma^2 g_v(x, x', s) = \delta(x - x'), \quad (5)$$

where $\gamma = \sqrt{(sL + R)(sC + G)}$, with $\text{Re}\{\gamma\} > 0$, and δ denotes the Dirac delta function. Once the voltage $V(x, s)$ is obtained, we obtain the time-domain voltage using the

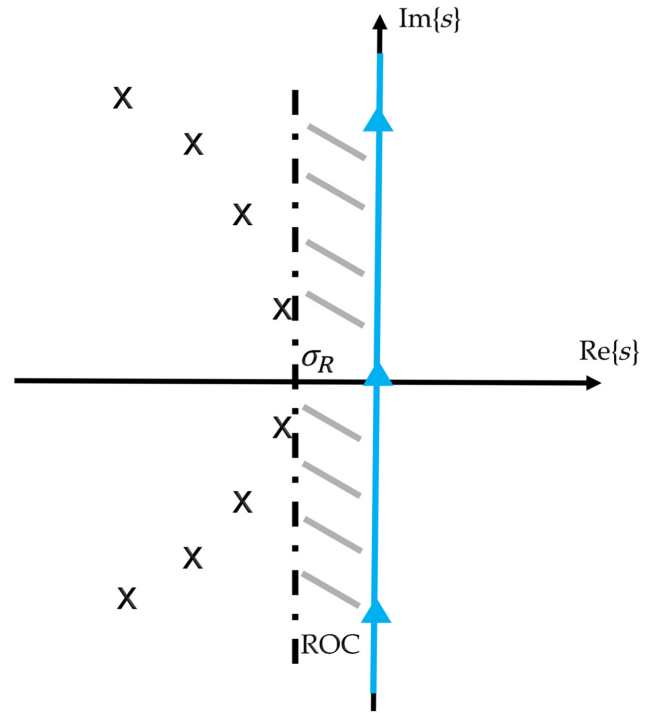


FIG. 2. Time-domain voltage is evaluated by taking the inverse Laplace transform along the imaginary axis. Here σ_R is the real part of the rightmost singularity of $V(x, s)$.

inverse Laplace transform:

$$V(x, t) = \frac{1}{2\pi j} \int_{\kappa - j\infty}^{\kappa + j\infty} V(x, s) e^{st} ds. \quad (6)$$

Here $-\sigma_R < \kappa < 0$ in the region of convergence (ROC), as shown in Fig. 2. In light of its realizability, our time-varying electromagnetic system is causal. Moreover, since it involves a single temporal switching, as opposed to periodic variation, it is necessarily stable. As a result, all the pole singularities of $V(x, s)$ must lie in the left side of the complex frequency plane ($\text{Re}\{s\} < 0$).

B. The spectral Green's function

The spectral Green's function $g_v(x, x', s)$ is obtained from Eq. (5) by following a standard procedure [52],

$$g_v(x, x', s) = \frac{F_v(x, x', s)}{W(s)}, \quad (7)$$

$$F_v(x, x', s) = \overleftarrow{u}(x^<) \overrightarrow{u}(x^>),$$

where $\overleftarrow{u}(x)$ [$\overrightarrow{u}(x)$] is the solution of the homogeneous equation corresponding to Eq. (5) that satisfies the boundary conditions on the left boundary, at $x = 0$, and on the right boundary, at $x = d$ (see Fig. 3), $x^< = \min(x, x')$, and $x^> = \max(x, x')$. Moreover, the Wronskian $W(s)$ that

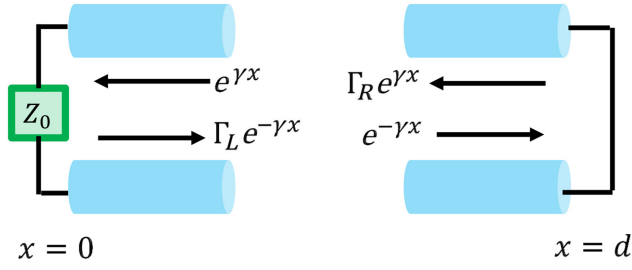


FIG. 3. Two terminated half-sided transmission line problems. By solving the two simple problems, Green's function is obtained.

tunes the discontinuity between the left and right solutions, $\overleftarrow{u}(x)$ and $\overrightarrow{u}(x)$, at the source location x' reads

$$W[\overleftarrow{u}, \overrightarrow{u}] = \overleftarrow{u}(x) \frac{d}{dx} \overrightarrow{u}(x) - \overrightarrow{u}(x) \frac{d}{dx} \overleftarrow{u}(x). \quad (8)$$

The homogeneous left and right solutions, i.e., $\overleftarrow{u}(x)$ and $\overrightarrow{u}(x)$, are expressed using simple Fresnel coefficients $\Gamma_{L,R}$:

$$\overleftarrow{u}(x) = e^{\gamma x} + \Gamma_L e^{-\gamma x}, \quad (9a)$$

$$\overrightarrow{u}(x) = e^{-\gamma x} + \Gamma_R e^{\gamma x}. \quad (9b)$$

Here $\Gamma_L(s) = [Z_0 - Z_2(s)]/[Z_0 + Z_2(s)]$ is the reflection coefficient at $x = 0$, where $Z_2(s) = \sqrt{(sL_2 + R_2)/(sC_2 + G_2)}$ is the characteristic impedance of the TL model of the layer *after* temporal switching. Note that the square root should be selected such that $\text{Re}\{Z_2\} > 0$, and $\Gamma_R = -e^{-2\gamma d}$. Next, by using Eqs. (9) in Eq. (8), the Wronskian is evaluated as

$$W(s) = -2\gamma(1 + \Gamma_L e^{-2\gamma d}). \quad (10)$$

By substituting Eqs. (9) and (10) into Eq. (7), the spectral domain Green's function is expressed as a sum of four wave contributions:

$$g_v(x, x', s) = [e^{-\gamma|x-x'|} - e^{\gamma(x+x'-2d)} + \Gamma_L e^{-\gamma(x+x')} - \Gamma_L e^{\gamma(|x-x'|-2d)}] / W(s). \quad (11)$$

Substituting Eq. (11) into Eq. (4) gives the spectral domain voltage $V(x, s)$.

Since the source term in Eq. (4), $f_s(x', s)$, is an analytic function, $g_v(x, x', s)$ and $V(x, s)$ share the same singular points in the complex s plane. Substituting the above obtained $V(x, s)$ into Eq. (6) yields the time-domain volt-

age at any point inside the TL model of the layer:

$$V(x, t) = \frac{1}{2\pi j} \int_{-j\infty}^{+j\infty} \frac{e^{st}}{W(s)} \int_{-\infty}^{\infty} F_v(x, x', s) f_{s,v}(x', s) dx' ds. \quad (12)$$

For completeness of the discussion, a similar procedure is applied to obtain the time-domain current $I(x, t)$ (see Appendix A).

IV. GOING BEYOND THE ROZANOV BOUND

We use the proposed time-variant approach to overcome Rozanov's bound for LTI systems with an ultrawideband as well as a quasimonochromatic signal, i.e., a modulated short time pulse. Recall that the Rozanov bound is formulated as [9]

$$|\ln \rho_0|(\lambda_{\max} - \lambda_{\min}) \leq 2\pi^2 \mu_s d, \quad (13)$$

where ρ_0 is the maximal reflection within the operating wavelength band $[\lambda_{\min}, \lambda_{\max}]$ and μ_s denotes the static permeability. Next, we demonstrate with a numerical example how this LTV approach may lead to bypassing Rozanov's bound.

In the following we apply the numerical procedure discussed above for the solution of pulsed wave scattering by a temporally switched layer. We select $t_s = 0$ as the switching moment where the pulse is located at the center of the layer. The excited voltage and current waves in the TL problem at $t = 0^-$ are considered in the form of a modulated Blackman-type function [53], and presented in Eq. (14) below. If there exist a phase difference between the baseband and the modulation terms, there will be several modulation frequencies on the ultrawideband regime where the average of the entire signal is close to zero. This implies that their frequency response is akin to a quasimonochromatic or narrowband signal. In our example, there is no such phase difference. We have

$$V_0(t) = \frac{1}{w} \sum_{k=0}^3 a_k \cos\left(\frac{2\pi k(v_p t - d/2)}{w}\right) \Pi_{T_p}\left(t - \frac{T_p}{2}\right) \times \cos\left(\frac{2\pi f_0(v_p t - d/2)}{v_p}\right), \quad (14)$$

where w is the pulse width within the layer, v_p is the wavefront propagation speed inside the layer before switching, the $\{a_k\}$ are Blackman's weighting coefficients, $f_0 = 1/T_0$ is the carrier frequency with T_0 being the time period of the carrier signal, and $\Pi_{T_p}(t) = H(t + T_p/2) - H(t - T_p/2)$, where $H(t)$ is the Heaviside function. We consider the pulse duration $T_p = w/v_p$. Using such notation, T_p/T_0 is a measure of the signal's fractional bandwidth. To clarify our notation, note that, with (i) $T_p/T_0 \rightarrow 0$, the signal is

practically a baseband signal while, with (ii) $T_p/T_0 \rightarrow \infty$, the signal is practically time harmonic. As T_p/T_0 increases in the range $0 < T_p/T_0 < \infty$, the signal's characteristics changes from those of an ultrawideband ($T_p/T_0 \lesssim O(1)$), to those of quasimonochromatic and narrowband.

For the demonstration, we consider the pulse temporal duration $T_p = 1.6$ ns. The physical layout is that of a layer with $d = 0.4$ m that is initially characterized by $\epsilon_1 = 1.5\epsilon_0$, $\mu_1 = \mu_0$, and $\sigma_1 = 0$, $\sigma_{m1} = 0$. At time $t = t_s$, while the pulse is tightly contained within the layer (i.e., $w \approx d$), the *permittivity and conductivity are simultaneously switched* to $\epsilon_2 = 0.75\epsilon_0$, $\sigma_2 > 0$, $\sigma_{m2} = 0$. We stress that the layer's permeability remains *unchanged* ($\mu_2 = \mu_0$), and, consequently, we *pump energy into the wave system* during the switching process.

Next, we evaluate the ratio of the *absorbed energy* in the layer to the incident energy for both time-variant and time-invariant layers, and for different values of T_p/T_0 . To that end, we make use of the reflected energy. The relation between the incident, reflected, and absorbed energies are given by

$$\frac{E_{\text{ref}}}{E_{\text{inc}}} = \frac{\int_{-\infty}^{\infty} |\rho_0(f) v_0(f)|^2 df}{\int_{-\infty}^{\infty} |v_0(f)|^2 df}, \quad \frac{E_{\text{abs}}}{E_{\text{inc}}} = 1 - \frac{E_{\text{ref}}}{E_{\text{inc}}}, \quad (15)$$

where $|v_0(f)|$ is the magnitude of the Fourier transform of the signal [$|v_0(f)| = |\text{FT}\{V_0(t)\}|$], E_{inc} , E_{ref} , and E_{abs} denote the incident, reflected, and absorbed energies, respectively. It should be noted that, generally, E_{ref} is composed of two contributions: (1) an early time ($t < t_s$) pulsed wave due to impedance mismatching at the layer's boundary and (2) a back reflected wave due to the switching of the TL parameters and the multiple wave bounces in the absorbing layer for $t > t_s$.

First, in the LTI case where the layer is time invariant and Rozanov's bound exists, the parameter ρ_0 in Eq. (13) is taken to maximize the left-hand side of Eq. (13) within the operating band to give

$$\rho_0 = \begin{cases} e^{-2\pi^2 \mu_s d / \Delta\lambda} & \text{if } \lambda \in [\lambda_{\text{min}}, \lambda_{\text{max}}], \\ 1 & \text{otherwise,} \end{cases} \quad (16)$$

where $\Delta\lambda = \lambda_{\text{max}} - \lambda_{\text{min}}$. Note that ρ_0 is a function of $\Delta\lambda$ that can be expressed by two frequency related parameters: a center frequency f_c and the bandwidth BW as follows: $\Delta\lambda = c_0 \text{BW} / [(f_c - \text{BW}/2)(f_c + \text{BW}/2)]$ and c_0 is the speed of light in vacuum. In order to minimize the reflection within the operating band, we perform a sweep of the parameters f_c and BW to maximize the ratio $E_{\text{abs}}/E_{\text{inc}}$ in Eq. (15). If the modulation frequency of the incident signal is much larger than its bandwidth, i.e., a narrowband signal, the optimal frequency will be equal to the modulation frequency. However, for quasimonochromatic and ultrawideband signals, this is not

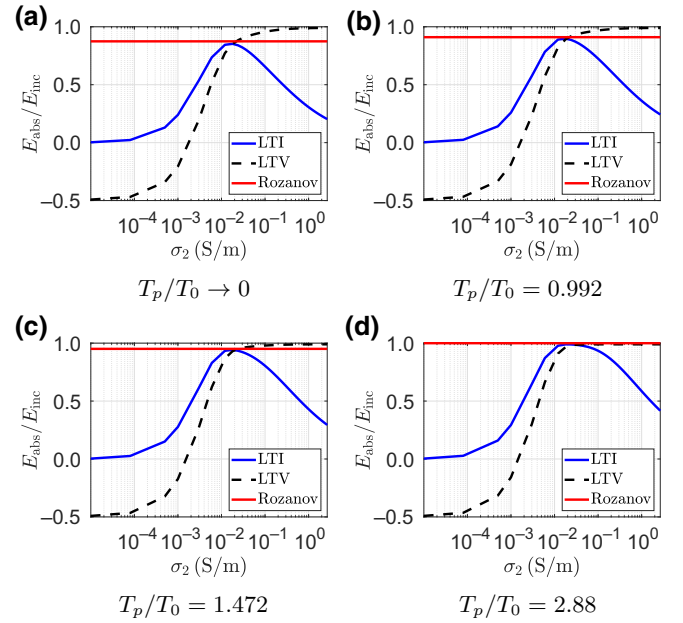


FIG. 4. Absorption caused by time-invariant and time-variant systems compared to Rozanov's bound as a function of the conductivity and for some values of the signal's frequency bandwidth.

always the case; therefore, a sweep along f_c and BW is performed.

In contrast, the absorbed energy of the *LTV system* is evaluated by subtracting the total reflected energy from the incident energy, i.e., $E_{\text{abs}} = E_{\text{inc}} - E_{\text{ref,initial}} - E_{\text{ref,s}}$, where $E_{\text{ref,initial}}$ is the initial reflected energy due to impedance mismatch before switching ($t_0 \leq t \leq t_0 + T_p$) and $E_{\text{ref,s}}$ denotes the total reflected energy after switching ($t > t_s$).

The absorption optimization results are presented in Fig. 4 as a function of the conductivity σ_2 for several values of $T_p/T_0 \in (0, 3)$ covering the range of extreme ultrawideband to quasimonochromatic signals. In Fig. 4, the red lines represent the proper Rozanov's bound, the blue lines represent a LTI system absorption response, and the black dashed lines are used to depict the absorption with the time-varying scheme. It can be observed in Fig. 4 that, for any given value of T_p/T_0 (signal bandwidth), it is possible to determine a range of conductivities σ_2 such that the time-varying scheme exhibits better, or at least equal, performance in comparison to Rozanov's bound. In particular, for certain bandwidth regimes, an enhanced performance of the time-varying scheme occurs for $\sigma \gtrsim 0.024$ [Figs. 4(a)–4(c)], while for other regimes, it asymptotically occurs for relatively larger values of the conductivity. Obviously, for the LTI case, shown with blue lines, the performance is always below the bound.

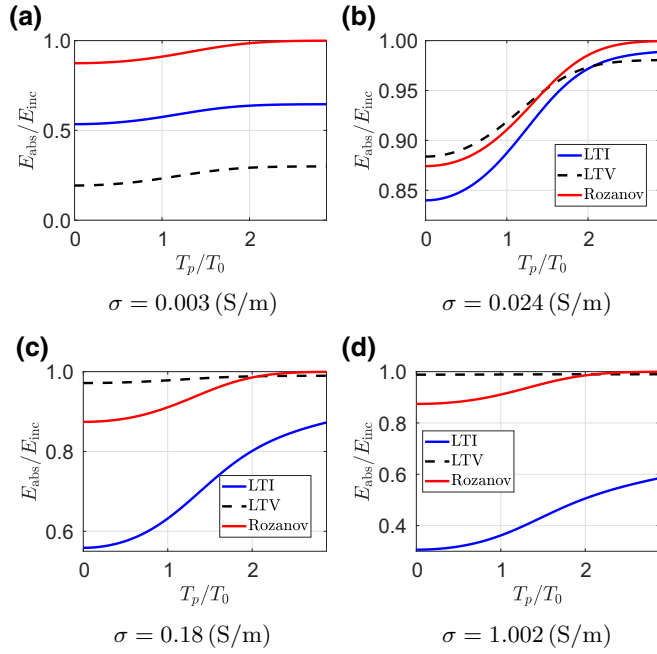


FIG. 5. Absorption caused by time-invariant and time-variant schemes compared to Rozanov’s bound as a function of the signal’s bandwidth and for some values of the conductivity.

A complementary view of the enhanced performances of the LTV scheme over Rozanov’s bound is demonstrated in Fig. 5, in which we plot the LTI, LTV, and Rozanov’s bounds using blue, dashed black, and red lines, respectively, for $\sigma_2 = 0.03, 0.054, 0.18, 1.002$ S/m as a function of the relative bandwidth T_p/T_0 . It can be easily noted from Fig. 5 that, for $\sigma_2 \gtrsim 0.024$ S/m, the LTV scheme performs better than Rozanov’s bounds in some bandwidth regimes of the excitation signal (for the parameters used here, $\sigma_2 \approx 0.024$ S/m can be identified as the minimal required value of loss for the LTV scheme in order to bypass the Rozanov’s bound for ultrawideband or quasimonochromatic signal excitation). This enhanced performance in terms of better absorption and extended bandwidth improves as σ_2 is moderately increased.

Finally, Fig. 6 depicts a contour plot (“isolines”) of the ratio between the absorbed energy of the LTV scheme and that predicted by the Rozanov’s bound, i.e.,

$$\frac{(E_{\text{abs}})|_{\text{LTV}}}{(E_{\text{abs}})|_{\text{Rozanov}}}.$$

Note that the results presented in Figs. 4 and 5 are obtained by horizontal and vertical “cuts” in Fig. 6 along Cartesian grid lines. Furthermore, the extent of the frequency bandwidth “windows” for which the LTV scheme bypasses the Rozanov bound are easily spotted by observing the regions in which the contour line height is larger than unity, i.e., $[(E_{\text{abs}})|_{\text{LTV}}/(E_{\text{abs}})|_{\text{Rozanov}} > 1]$ for $\sigma_2 \gtrsim$

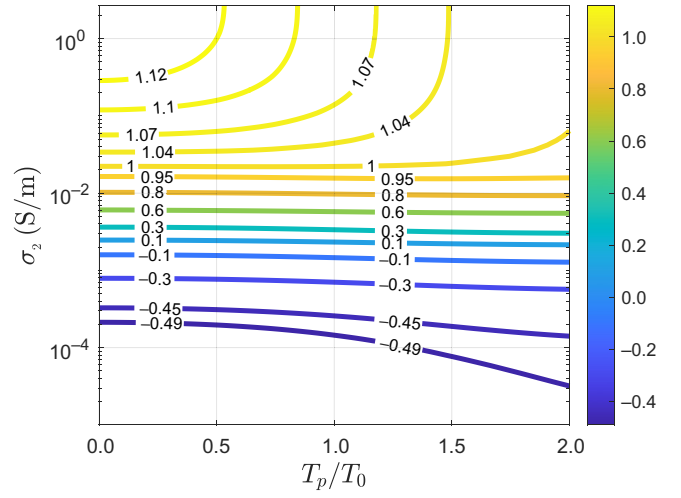


FIG. 6. A contour plot (“isolines”) of the ratio of the absorbed energy of the LTV scheme to that predicted by Rozanov’s bound, i.e., $(E_{\text{abs}})|_{\text{LTV}}/(E_{\text{abs}})|_{\text{Rozanov}}$ [see in Eq. (15)].

0.024 and $T_p/T_0 < 1.9$, while for $T_p/T_0 > 1.9$, it asymptotically approaches 1. The negative values in Fig. 6 for low values of conductivity (σ_2) are due to energy injection into the wave system during switching. Therefore, the reflected field is stronger than the incident field and can be recognized as negative absorption. To conclude the discussion, this example demonstrates that Rozanov’s absorption bound is valid only for LTI systems, and can be bypassed for certain cases by utilizing mechanisms due to time variation; moreover, the example demonstrates the appealing characteristics of the time-varying scheme that involve *permittivity and conductivity (material loss) switching* for ultrawideband and quasimonochromatic as well as narrowband (time harmonic) signals. In order to reduce the “break-even” points for which Rozanov’s bound bypasses the LTV scheme in Fig. 5, and to further lower the required minimal σ_2 values, it may be beneficial to use the more complex time-variation schemes that involve, besides permittivity and conductivity switching, switching of the material permeability.

The bounds demonstrated in this discussion are evaluated using the absorbed energy spectrum of the signal along the *entire frequency band* [note that $f \in (-\infty, \infty)$ in Eq. (15)]. It should be recalled that switching the medium permeability and permittivity changes the pulse temporal width and consequently its frequency spectrum [10]. Therefore, if interest is only, for example, in the minimization of the power reflection in the frequency band of the incident wave, while discarding the reflection outside this band, then the time switching of the permittivity only can be applied such that parts of the frequency spectrum are disperse to other bands outside that of the incident

wave. Such an effect is utilized and nicely discussed in Ref. [13] for quasimonochromatic signals.

V. REALISTIC IMPLEMENTATION

In the previous section we demonstrated a theoretical way to bypass Rozanov's bound by performing an abrupt switching of both conductivity and permittivity of the dielectric layer. There are however two important challenges with this scheme. First, we have to design a metamaterial and an as simple as possible switching scheme that will change the effective properties (conductivity and permittivity) between the values suggested in Sec. IV. Second, abrupt switching is impractical, and may even contradict causality, and therefore it is essential to demonstrate that the proposed scheme to bypass Rozanov's bound also applies with gradual switching. These issues are addressed below.

A. Effective media

Here, we suggest a practical system that realizes the transition $\{\epsilon_1 = 1.5\epsilon_0, \sigma_1 = 0\}$ to $\{\epsilon_2 = 0.75\epsilon_0, \sigma_2 = 0.18 \text{ S/m}\}$ demonstrated in Fig. 5(c). Such an extreme transition between a pure dielectric material to an absorbing material with high losses requires a variation of the topology of the metamaterial during switching. It can be achieved by altering a 3D system to a 2D system. As previously shown, this transition achieves $(E_{\text{abs}})_{\text{LTV}}/(E_{\text{abs}})_{\text{Rozanov}} > 1$ for an increased range of modulated pulses. We use a metamaterial structure that is composed of cubical unit cells with unit cell size a . Each cell contains a PEC wire (dipole) with the length of each arm denoted by l and the resistor length denoted by l_R . The total dipole length is $2l + l_R$, and this should be equal to a since a is the cubical unit cell size. The dipole's diameter is denoted by $2r_0$ loaded with a resistor R between its two terminals (see Fig. 7). We obtain the required effective properties (ϵ_1, σ_1) , (ϵ_2, σ_2) by proper selection of the dimensions of the wires and the resistance [54–56]. We consider the following parameters: $a = 20 \text{ mm}$, $r_0 = 0.846 \text{ mm}$, $l_R = 7.4 \text{ mm}$. The wires are located in a host dielectric media with $\epsilon_h = 1.3$ (such as CarbonFoam PU 2 R PU [57]).

Effective media characteristics before switching are $\epsilon_1 = 1.5\epsilon_0, \sigma_1 = 0$. Here, an open circuit ($R \rightarrow \infty$) is enforced between the two terminals, so the electric polarizability of a single wire is given by $\alpha_{ee} = l^2/(j2\pi fZ_{\text{wire}})$, where the input impedance of the wire Z_{wire} is given by [54,58]

$$Z_{\text{wire}} = \frac{\eta_0 \Psi_{\text{dr}}}{2\pi j \{1 + k^2 l^2 F/3 - jk^3 l^3/[3(\Omega - 3)]\}}, \quad (17)$$

where the dimensionless parameters are $F = 1 + 1.08/(\Omega - 3)$, $\Omega = 2 \ln(2l/r_0)$, and $\Psi_{\text{dr}} = 2 \ln(l/r_0) - 2$. The

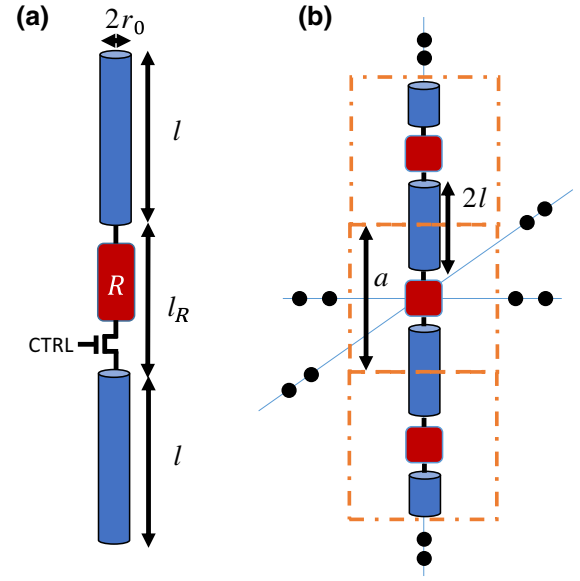


FIG. 7. Metamaterial topology. (a) Each element is composed of a dipole connected by a resistor in its two terminals. The dipole has a total length of $2l$ and a thickness of $2r_0$. The length of the resistor R is l_R . The switching device is composed of a single CMOS transistor with a controlling feature (CTRL). (b) Each unit cell (sized a) is attached to its neighbors vertically. By changing the resistance to a finite value, the current flows vertically across the unit cells, thus altering the 3D system to a 2D system.

dipole polarizability in free space should satisfy the radiation condition, and therefore a radiation correction should be taken into account. However, for a nonresonant quasi-static metamaterial, such a correction will produce a minor impact on the effective properties, since $|\text{Re}(\alpha)| \gg |\text{Im}(\alpha)|$ (see Appendix B for further discussion). Applying the electric polarizability α_{ee} with the Maxwell Garnett homogenization procedure [56] for 3D structures provides the analytic complex effective permittivity

$$\epsilon_{\text{eff}} = \epsilon_0 \epsilon_h + N \alpha_{ee} \left(1 - \frac{N \alpha_{ee}}{3 \epsilon_0 \epsilon_h}\right)^{-1}, \quad (18)$$

where $N = 1/a^3$ denotes the lattice density. Using this analytical formalism with $l = 0.0085 \text{ m}$ provides $\epsilon_{\text{eff}} \sim \epsilon_1$. In order to verify and fine tune the analytic results, we use high-frequency simulation software (HFSS) [59] to extract the effective parameters of the homogenized slab. We use a well-known extraction technique [60] that uses the scattering (\bar{S}) parameters of a normal incidence illumination (see Fig. 8 for the simulation setup). A postprocessing deembedding is performed to obtain the \bar{S} parameters at the interface between the slab and the vacuum (marked by blue dashed arrows). By the simulation optimization, the following design parameters are obtained in order to fit with the desired effective material properties before switching: $l = 0.0063 \text{ m}$, $R = 300 \text{ G}\Omega$. Because of edge effects, there

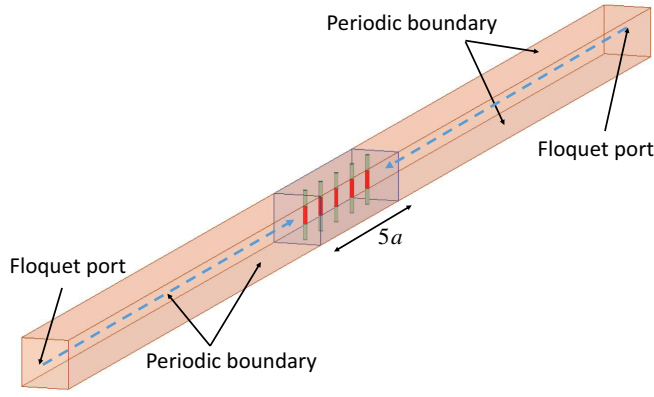


FIG. 8. HFSS simulation setup. The periodic structure (periodic boundary conditions) is excited by a Floquet port where only the fundamental mode is propagating. By evaluating the \tilde{S} parameters and by performing a postprocessing deembedding we extract the effective properties of the discrete slab.

is a slight deviation between the optimal dipole length compared to the analytical formulas that is expectable under real design considerations.

Results are presented in Figs. 9(a) and 9(b) with the standard definition of the relative permittivity, $\epsilon_r = \epsilon_{\text{eff}}/\epsilon_0$, and $\epsilon_r = \epsilon'_r - j\sigma/(2\pi f\epsilon_0)$, where ϵ'_r denotes the real part of ϵ_r . *Effective media characteristics after switching* are $\epsilon_2 = 0.75\epsilon_0$, $\sigma_2 = 0.18$ S/m. Here, we use a 2D homogenization procedure suggested in Ref. [55] that was developed for a loaded wire structure,

$$\epsilon_{\text{eff}} = \epsilon_0 \epsilon_h - \frac{1}{\omega^2 a^2 \tilde{L} - j\omega a^2 \tilde{R}}, \quad (19)$$

where $\tilde{L} = [\mu_0/(2\pi)] \ln\{a^2/[4r_0(a-r_0)]\}$ and $\tilde{R} = R/a\Omega/\text{m}$ are the inductance and resistance per unit length, respectively. In this case, the optimal performances to obtain a homogenized medium with $\epsilon_2 = 0.75\epsilon_0$, $\sigma_2 = 0.18$ S/m are obtained with $R = 272 \Omega$ in the theoretical calculations, and $R = 264 \Omega$ extracted using numerical HFSS optimization. The theoretical calculations assume a lumped resistor, while the simulation also takes into account the dimensions of the resistor. Results are presented in Figs. 9(c) and 9(d). During switching between the two states only the resistance is altered, so by using a switch as shown in Fig. 7(a), this switch, during the transition from open to closed, alters the nature of the metastructure system from 3D to 2D. This change enables us to obtain lower values of ϵ ($\epsilon_2 < \epsilon_1$), while considering an additional loss mechanism (σ_2). Excellent agreement between the desired, analytical, and extracted effective parameters both before and after switching is provided by this scheme, as can be observed in Fig. 9. To conclude the discussion, both analytical and numerical calculations show that a dipole-based metamaterial can exhibit the

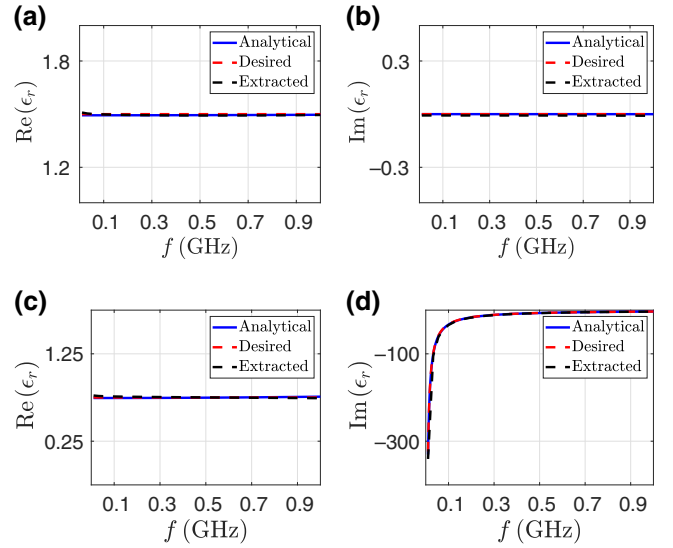


FIG. 9. Analytical, desired, and extracted complex ϵ as a function of the frequency f (a),(b) before switching and (c),(d) after switching.

required effective media properties for the design of an absorbing material with better performance than that of Rozanov's bound.

B. Gradual switching

In Sec. IV we demonstrated how the Rozanov bound can be bypassed by using an abrupt switching of the effective parameters. Such a switching scheme may be challenging practically and may even contradict causality. Therefore, we consider here a gradual (soft) switching scenario that lasts over an extended period of time, even larger than the temporal width of the impinging pulse. The switching process begins at $t = 0$, while the pulse is contained within the layer and ends at some time $t_s > 0$ (see Fig. 10). In a previous work [38] using WKB analysis some of the authors of this paper have showed the equivalence of soft switching and the staircase approximation. Hence, here, gradual switching is implemented as a series of “small sized” abrupt switchings (staircase steps), where the values of the permittivity and conductivity change.

In each time step, we evaluate numerically the voltage and current along the TL using the initial conditions obtained in the previous step and by considering the effect of the abrupt voltage change due to switching (see Sec. III). Generally, at each of the small switching steps we require the continuity of the magnetic flux and the electric charge on the TL section that undergoes switching at $x > 0^+$, and, consequently, the continuity of the voltage and current there is obviously not satisfied. We stress, however, that at $x = 0^+$, at the connection point between the TL sections in $x > 0$ and $x < 0$, this continuity condition does not hold.

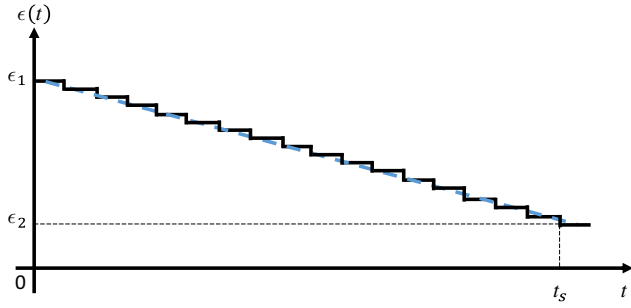


FIG. 10. Illustration of gradual (soft) switching. The switching process begins at $t = 0$ and ends at t_s . It is implemented as a series of “small sized” abrupt switchings, with constant step durations (black). The continuous limit is shown as a dashed blue line.

Instead, at $x = 0^+$, we enforce the continuity of the voltage and the current. This is essential because the properties of the TL section at $x < 0$ are unaltered during the entire switching process, implying that the current and voltage on it also remain continuous at each one of the switching steps. Thus, at $x = 0$ at any switching moment we have

$$\begin{aligned} I'_0(0) &= \lim_{h \downarrow 0} \frac{I_0(h) - V_0(0)/Z_0}{h}, \\ V'_0(0) &= \lim_{h \downarrow 0} \frac{V_0(h) - Z_0 I_0(0)}{h}. \end{aligned} \quad (20)$$

Note that in the example the current remains continuous since the magnetic properties are unchanged. We emphasize that, for the gradual switching process (unlike a single abrupt switching), one must evaluate both the voltage and the current in each step, since they are used to evaluate the initial conditions for the next switching (I_0 and V_0).

Here, we consider the transition $\{\epsilon_1 = 1.5\epsilon_0, \sigma_1 = 0\}$ to $\{\epsilon_2 = 0.75\epsilon_0, \sigma_2 = 0.18 \text{ S/m}\}$ for $T_p/T_0 = 0.992$ [compare to Fig. 4(b) for a single abrupt switching], with the parameters obtained in the metamaterial realization that was discussed in Sec. V A. The absorption results are presented in Fig. 11 for several time step values (blue line, $0.25T_p$; red line, $0.375T_p$; yellow line, $0.5T_p$; and purple line, $0.625T_p$). It can be seen from Fig. 11 that, for switching times that are of the order of, and even larger than, the pulse temporal width $t_s < 10T_p$, the time-variant system provides better performance compared to Rozanov’s bound. Obviously, as the switching time tends to infinity, the system is not time varying anymore; it remains at its first state where the slab is lossless with $\epsilon_1 = 1.5\epsilon_0$, and therefore its absorption is zero, as expected, and shown in Fig. 11. Remarkably, even switching of 5 times the pulse width leads to a minor effect on the performance, and, interestingly, gradual switching may lead to better performance even when compared to the case of abrupt switching. This is a consequence of the reduced reflection

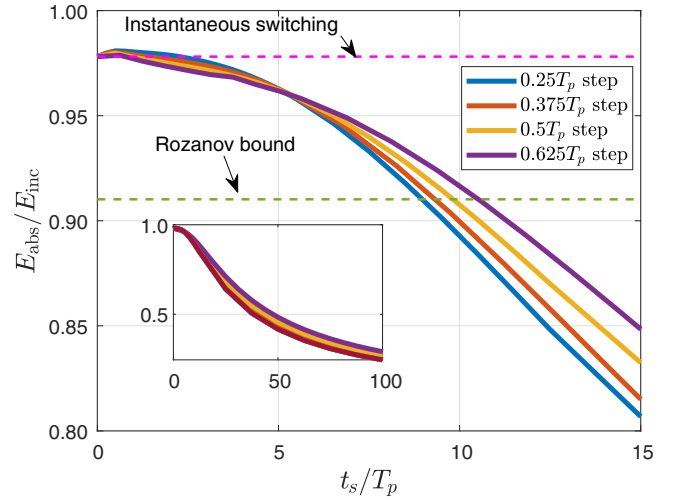


FIG. 11. Switching is performed gradually in a staircase manner. In each step, the permittivity and conductivity are abruptly switched. Time steps are $0.25T_p$ (blue line), $0.375T_p$ (red line), $0.5T_p$ (yellow line), and $0.625T_p$ (purple line). Remarkably, the time-varying absorber under gradual switching performs similarly to what is expected by instantaneous switching, and even better under certain conditions. As the switching time extends above approximately $10T_p$, eventually, the time invariance does not introduce an improvement compared with the Rozanov bound for LTI absorbers.

coefficient caused by a gradual time switching, in comparison to that caused by an instantaneous switching [38]. Consequently, in light of the possibility of using switching times that are substantially larger than the pulse temporal width, the pulse in these cases may be either fully or only partially contained within the layer at $t = 0$, as the switching process starts, with no substantial degradation in performance, thus increasing the tolerance in the switching process.

VI. SUMMARY AND CONCLUSION

In this manuscript, we consider the problem of a short pulse propagating and scattering from an electromagnetic wave absorber with time-varying properties. A transmission line equivalent is used to formulate an initial boundary problem. The problem is solved by finding the spectral (on the Laplace s plane) Green’s function, followed by an inverse Laplace transform. This formalism is used to obtain the time-domain-reflected voltage and current from which all other required quantities are calculated. Using this numerical procedure, we solve the problem of reflection by a dielectric layer absorber in which the permittivity and conductance are switched in time. We further demonstrate that Rozanov’s LTI absorption bound, when calculated over the *whole signal’s spectrum range*, can be bypassed for modulated pulsed signals, ultrawideband, quasimonochromatic, and narrowband, by such

abrupt switching. We present a time-dependent switchable metamaterial structure that exhibits the required effective media properties before and after switching. Furthermore, we examine a gradual switching that also results in an improved performance compared to Rozanov's bound, similar, and even better than what is expected when using an idealistic instantaneous switching.

ACKNOWLEDGMENTS

C.F. acknowledges support from the Darom Scholarship, the High-tech, Bio-tech, and Chemo-tech Scholarship, and the Yaakov Ben-Yitzhak Hacohen excellence Scholarship. This research is supported by the Israel Science Foundation (Grant No. 1353/19).

APPENDIX A: TIME-DOMAIN CURRENT

The spectral domain Helmholtz equation for the current in a lossy medium can be written as

$$\frac{\partial^2 I(x, s)}{\partial x^2} - \gamma^2 I(x, s) = f_{s,i}(x, s), \quad (\text{A1a})$$

$$f_{s,i}(x, s) = C \frac{\partial V_0(x)}{\partial x} - L(sC + G)I_0(x), \quad (\text{A1b})$$

where γ is the complex propagation term and L, C, R, G are the TL inductance, capacitance, series resistance, and shunt admittance per unit length, respectively. Green's function for the current term is obtained in similarly to the voltage (see Sec. III):

$$g_i(x, x', s) = \frac{F_i(x, x', s)}{W(s)}, \quad (\text{A2a})$$

$$F_i(x, x', s) = e^{-\gamma|x-x'|} + e^{\gamma(x+x'-2d)} - \Gamma_L e^{-\gamma(x+x')} - \Gamma_R e^{\gamma(x-x'-2d)}. \quad (\text{A2b})$$

Here $W(s)$ is the Wronskian term [see Eq. (10)]. The time-domain current at any point inside the TL is obtained by performing an inverse Laplace transform, upon changing F_v and $f_{s,v}$ by F_i and $f_{s,v}$ in Eq. (12).

APPENDIX B: RADIATION CORRECTION OF THE POLARIZABILITY

Energy conservation implies that in the absence of material loss, the complex polarizability satisfies the radiation condition $\text{Im}(1/\alpha) = k^3/6\pi\epsilon_0$ [55]. Let us denote the polarizability term discussed in Sec. V A by $\alpha_{ee} = \alpha_{\text{uncorrected}}$, since it does not stand under this condition. The

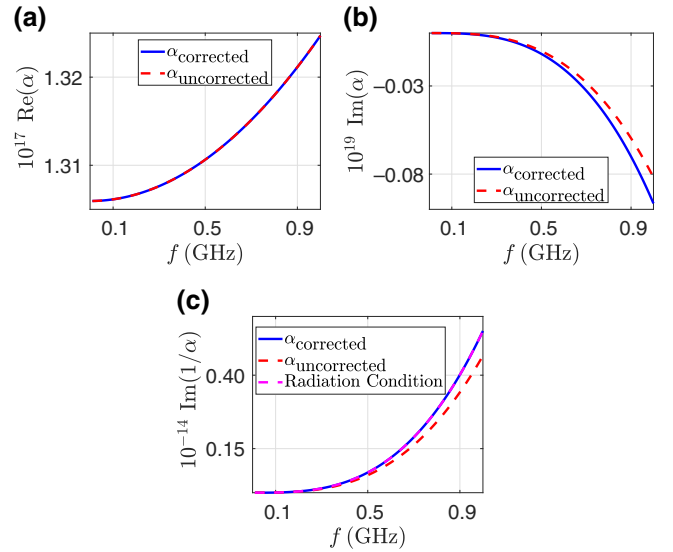


FIG. 12. Corrected and uncorrected polarizability coefficients: (a) real part, (b) imaginary part, (c) radiation condition.

radiation correction X is given by

$$X = k^3/6\pi\epsilon_0 - \text{Im}(1/\alpha_{\text{uncorrected}}). \quad (\text{B1})$$

The corrected polarizability is defined as

$$\alpha_{\text{corrected}} = \frac{\alpha_{\text{uncorrected}}}{1 + jX\alpha_{\text{uncorrected}}}. \quad (\text{B2})$$

It is immediate to verify that $\alpha_{\text{corrected}}$ satisfies the radiation condition. In Fig. 12 we compare the corrected and uncorrected coefficients. We note that $\text{Re}(\alpha_{\text{corrected}}) \approx \text{Re}(\alpha_{\text{uncorrected}})$ since $|\text{Re}(\alpha_{\text{uncorrected}})| \gg |\text{Im}(\alpha_{\text{uncorrected}})|$; however, the imaginary part is different, which compensates for the radiation condition.

- [1] A. Li, S. Singh, and D. Sievenpiper, Metasurfaces and their applications, *Nanophotonics* **7**, 989 (2018).
- [2] X. Luo, Subwavelength artificial structures: Opening a new era for engineering optics, *Adv. Mater.* **31**, 1804680 (2019).
- [3] N. I. Landy, S. Sajuyigbe, J. J. Mock, D. R. Smith, and W. J. Padilla, Perfect Metamaterial Absorber, *Phys. Rev. Lett.* **100**, 207402 (2008).
- [4] W. Li and J. Valentine, Metamaterial perfect absorber based hot electron photodetection, *Nano Lett.* **14**, 3510 (2014).
- [5] G. Ruck, *Radar Cross Section Handbook: Volume 1*, (Springer, New York, NY, 1970), Vol. 1.
- [6] Y.-J. Park, A. Herschlein, and W. Wiesbeck, A photonic bandgap (pbg) structure for guiding and suppressing surface waves in millimeter-wave antennas, *IEEE Trans. Microw. Theory Tech.* **49**, 1854 (2001).
- [7] S. Qu, Y. Hou, and P. Sheng, Conceptual-based design of an ultrabroadband microwave metamaterial absorber, *National Acad. Sci.* **118**, (2021).

- [8] Y. Li and B. M. Assouar, Acoustic metasurface-based perfect absorber with deep subwavelength thickness, *Appl. Phys. Lett.* **108**, 063502 (2016).
- [9] K. N. Rozanov, Ultimate thickness to bandwidth ratio of radar absorbers, *IEEE Trans. Antennas Propag.* **48**, 1230 (2000).
- [10] A. Shlivinski and Y. Hadad, Beyond the Bode-Fano Bound: Wideband Impedance Matching for Short Pulses Using Temporal Switching of Transmission-Line Parameters, *Phys. Rev. Lett.* **121**, 204301 (2018).
- [11] H. Li, A. Mekawy, and A. Alù, Beyond Chu's Limit with Floquet Impedance Matching, *Phys. Rev. Lett.* **123**, 164102 (2019).
- [12] X. Guo, H. Lissek, and R. Fleury, Improving Sound Absorption through Nonlinear Active Electroacoustic Resonators, *Phys. Rev. Appl.* **13**, 014018 (2020).
- [13] H. Li and A. Alù, Temporal switching to extend the bandwidth of thin absorbers, *Optica* **8**, 24 (2020).
- [14] D. M. Solís and N. Engheta, Functional analysis of the polarization response in linear time-varying media: A generalization of the kramers-kronig relations, *Phys. Rev. B* **103**, 144303 (2021).
- [15] P.-Y. Chen, C. Argyropoulos, and A. Alù, Broadening the Cloaking Bandwidth with Non-Foster Metasurfaces, *Phys. Rev. Lett.* **111**, 233001 (2013).
- [16] C. Caloz and Z.-L. Deck-Léger, Spacetime metamaterials—part i: General concepts, *IEEE Trans. Antennas Propag.* **68**, 1569 (2019).
- [17] C. Caloz and Z.-L. Deck-Léger, Spacetime metamaterials—part ii: Theory and applications, *IEEE Trans. Antennas Propag.* **68**, 1583 (2019).
- [18] S. Y. Elnaggar and G. N. Milford, Modelling space-time periodic structures with arbitrary unit cells using time periodic circuit theory, *IEEE Trans. Antennas Propag.* (2020).
- [19] S. Taravati and G. V. Eleftheriades, Generalized Space-Time-Periodic Diffraction Gratings: Theory and Applications, *Phys. Rev. Appl.* **12**, 024026 (2019).
- [20] Z.-L. Deck-Léger, N. Chamanara, M. Skorobogatiy, M. G. Silveirinha, and C. Caloz, Uniform-velocity spacetime crystals, *Adv. Photonics* **1**, 056002 (2019).
- [21] Y. Hadad, D. L. Sounas, and A. Alù, Space-time gradient metasurfaces, *Phys. Rev. B* **92**, 100304 (2015).
- [22] N. Chamanara, Y. Vahabzadeh, and C. Caloz, Simultaneous control of the spatial and temporal spectra of light with space-time varying metasurfaces, *IEEE Trans. Antennas Propag.* **67**, 2430 (2019).
- [23] H. B. Sedeh, M. M. Salary, and H. Mosallaei, Time-varying optical vortices enabled by time-modulated metasurfaces, *Nanophotonics* **1**, 2957 (2020).
- [24] S. Taravati and G. V. Eleftheriades, Full-Duplex Nonreciprocal Beam Steering by Time-Modulated Phase Gradient Metasurfaces, *Phys. Rev. Appl.* **14**, 014027 (2020).
- [25] H. Barati Sedeh, M. M. Salary, and H. Mosallaei, Topological Space-Time Photonic Transitions in Angular-Momentum-Biased Metasurfaces, *Advanced Optical Materials*, 2000075 (2020).
- [26] H. B. Sedeh, M. M. Salary, and H. Mosallaei, Adaptive multichannel terahertz communication by space-time shared aperture metasurfaces, *IEEE Access* **8**, 185919 (2020).
- [27] M. F. Imani, D. R. Smith, and P. del Hougne, Perfect absorption in a disordered medium with programmable meta-atom inclusions, *Adv. Funct. Mater.* **30**, 2005310 (2020).
- [28] Y. Shi and S. Fan, Dynamic non-reciprocal meta-surfaces with arbitrary phase reconfigurability based on photonic transition in meta-atoms, *Appl. Phys. Lett.* **108**, 021110 (2016).
- [29] V. Pacheco-Peña and N. Engheta, Antireflection temporal coatings, *Optica* **7**, 323 (2020).
- [30] H. Kazemi, M. Y. Nada, T. Mealy, A. F. Abdelshafy, and F. Capolino, Exceptional Points of Degeneracy Induced by Linear Time-Periodic Variation, *Phys. Rev. Appl.* **11**, 014007 (2019).
- [31] H. Kazemi, A. Hajiaghajani, M. Y. Nada, M. Dautta, M. Alshetaiwi, P. Tseng, and F. Capolino, Ultra-sensitive radio frequency biosensor at an exceptional point of degeneracy induced by time modulation, *IEEE Sens. J.* **21**, 7250 (2020).
- [32] K. Rouhi, H. Kazemi, A. Figotin, and F. Capolino, Exceptional points of degeneracy directly induced by space-time modulation of a single transmission line, *IEEE Antennas Wireless Propag. Lett.* **19**, 1906 (2020).
- [33] Y. Hadad and A. Shlivinski, in *2020 IEEE International Symposium on Antennas and Propagation and North American Radio Science Meeting* (IEEE, 2020), p. 1633.
- [34] P. Lohmannia and M. Manteghi, Broadband Parametric Impedance Matching for Small Antennas Using the Bode-Fano Limit: Improving on Chu's Limit for Loaded Small Antennas, *IEEE Antennas Propag. Mag.* (2021).
- [35] Y. Xiao, G. P. Agrawal, and D. N. Maywar, Spectral and temporal changes of optical pulses propagating through time-varying linear media, *Opt. Lett.* **36**, 505 (2011).
- [36] Y. Xiao, D. N. Maywar, and G. P. Agrawal, Reflection and transmission of electromagnetic waves at a temporal boundary, *Opt. Lett.* **39**, 574 (2014).
- [37] K. Tan, H. Lu, and W. Zuo, Energy conservation at an optical temporal boundary, *Opt. Lett.* **45**, 6366 (2020).
- [38] Y. Hadad and A. Shlivinski, Soft temporal switching of transmission line parameters: Wave-field, energy balance, and applications, *IEEE Trans. Antennas Propag.* **68**, 1643 (2020).
- [39] T. T. Koutserimpas and R. Fleury, Electromagnetic fields in a time-varying medium: Exceptional points and operator symmetries, *IEEE Trans. Antennas Propag.* (2020).
- [40] K. A. Lurie, D. Onofrei, W. C. Sanguinet, S. L. Weekes, and V. V. Yakovlev, Energy accumulation in a functionally graded spatial-temporal checkerboard, *IEEE Antennas Wirel. Propag. Lett.* **16**, 1496 (2017).
- [41] K. A. Lurie and V. V. Yakovlev, Energy accumulation in waves propagating in space-and time-varying transmission lines, *IEEE Antennas Wirel. Propag. Lett.* **15**, 1681 (2016).
- [42] M. S. Mirmoosa, G. Ptitsyn, V. S. Asadchy, and S. Tretyakov, Time-Varying Reactive Elements for Extreme Accumulation of Electromagnetic Energy, *Phys. Rev. Appl.* **11**, 014024 (2019).
- [43] Y. Kiasat, V. Pacheco-Peña, B. Edwards, and N. Engheta, in *CLEO: Science and Innovations* (Optical Society of America, 2018), p. JW2A-90.
- [44] T. T. Koutserimpas and R. Fleury, Electromagnetic waves in a time periodic medium with step-varying

- refractive index, *IEEE Trans. Antennas Propag.* **66**, 5300 (2018).
- [45] Y. Hadad and D. Sounas, Space-time modulated loaded-wire metagratings for magnetless nonreciprocity and near-complete frequency conversion, arXiv preprint [ArXiv:1906.00215](https://arxiv.org/abs/1906.00215) (2019).
- [46] M. S. Mirmoosa, G. A. Ptitycyn, R. Fleury, and S. Tretyakov, Instantaneous radiation from time-varying electric and magnetic dipoles, *Phys. Rev. A* **102**, 013503 (2020).
- [47] G. Ptitycyn, M. S. Mirmoosa, and S. A. Tretyakov, Time-modulated meta-atoms, *Phys. Rev. Res.* **1**, 023014 (2019).
- [48] M. Mirmoosa, T. Koutserimpas, G. Ptitycyn, S. Tretyakov, and R. Fleury, Dipole polarizability of time-varying particles, arXiv preprint [ArXiv:2002.12297](https://arxiv.org/abs/2002.12297) (2020).
- [49] R. E. Collin, *Foundations for Microwave Engineering* (McGraw-Hill, New York, 1966).
- [50] N. N. Rao, *Elements of Engineering Electromagnetics* (University of Illinois at Urbana-Champaign, NJ, USA, 2004).
- [51] However, a special case occurs when $L_1/C_1 = L_2/C_2$, where only a single propagating wave will be generated.
- [52] L. B. Felsen and N. Marcuvitz, *Radiation and Scattering of Waves*, (John Wiley & Sons, Hoboken, NJ, USA, 1994), Vol. 31.
- [53] A. Nuttall, Some windows with very good sidelobe behavior, *IEEE Trans. Acoust.* **29**, 84 (1981).
- [54] A. Serdyukov, I. Semchenko, S. Tretyakov, and A. Sihvola, *Electromagnetics of Bi-Anisotropic Materials: Theory and Applications* (Gordon and Breach, Amsterdam, The Netherlands, 2001).
- [55] S. Tretyakov, *Analytical Modeling in Applied Electromagnetics* (Artech House, MA, USA, 2003).
- [56] S. Tretyakov and F. Mariotte, Maxwell garnett modeling of uniaxial chiral composites with bianisotropic inclusions, *J. Electromagnetic Waves Appl.* **9**, 1011 (1995).
- [57] CarbonFoam PU 2 R PU material can be found at: <http://www.matweb.com/search/DataSheet.aspx?MatGUID=d0d331e36b884b71811b86321de93987>. However, additional similar materials can be found at: <http://www.matweb.com/search/PropertySearch.aspx>.
- [58] R. WP. King and C. Harisson, *Antennas and Waves: a Modern Approach* (MIT Press, MA, USA, 1969).
- [59] www.ansys.com.
- [60] D. R. Smith, S. Schultz, P. Markoš, and C. M. Soukoulis, Determination of effective permittivity and permeability of metamaterials from reflection and transmission coefficients, *Phys. Rev. B* **65**, 195104 (2002).